Ceramics International 50 (2024) 12549–12556

Contents lists available at ScienceDirect

Ceramics International

journal homepage: www.elsevier.com/locate/ceramint

Mechanisms for optimizing the dielectric properties of spinel $Li_{10}ZnTi_{13}O_{32}$ ceramics by Na^{+} doping

Haotian Liu [a], Kui Liu [a,*], Da Huang [a], Qin Yu [a], Cheng Liu [a], Jie Li [a], Yulong Liao [a], Dainan Zhang [a,b,**], Huaiwu Zhang [a,c,***]

[a] School of Electronic Science and Engineering, University of Electronic Science and Technology of China, Chengdu, 610054, China
[b] School of Integrated Circuit Science and Engineering, University of Electronic Science and Technology of China, Chengdu, China
[c] State Key Laboratory of Electronic Thin Film and Integrated Devices, University of Electronic Science and Technology of China, Chengdu 610054, China

ARTICLE INFO

Handling editor: P. Vincenzini

Keywords:
First-principles
$Li_{(1-x)10}Na_{10x}ZnTi_{13}O_{32}$
Microwave dielectric properties
Lattice vibration

ABSTRACT

Herein, the dielectric properties of Na^{+} doped $Li_{10}ZnTi_{13}O_{32}$ ceramics were investigated by first-principles computational prediction and combined with the solid-phase reaction method. $Li_{9.88}Na_{0.12}ZnTi_{13}O_{32}$ obtained the best dielectric properties by sintering at 1050 °C for 4 h: $\varepsilon_r = 30.01$, $Q \times f = 90{,}879$ GHz (@7.8 GHz), $\tau_f = 3.93$ ppm/°C. In terms of extrinsic factors, the optimization of the densification, the creation of the second phase TiO_2, and the increase of the grain size resulted in better dielectric properties. Intrinsic factors indicate that the weakening of the damping behavior and the increase in the electron cloud density lead to a decrease in the dielectric loss. The increase in ion polarisation and the blue shift of the Raman wavenumber lead to a gradual increase in ε_r. The temperature stability is optimized depending on the TiO_2 content. The optimized $Li_{9.88}Na_{0.12}ZnTi_{13}O_{32}$ ceramics have unlimited applications in microwave communications.

1. Introduction

With the high-speed development of fifth-generation communication technology, microwave dielectric ceramics (MWDCs) as the substrate material for passive electronic devices in microwave communication has also received extensive attention. In particular, electronic devices such as filters, resonators, antennas, duplexers, etc. are developing in the direction of miniaturization, lightweight, and high integration, which has prompted the need for microwave dielectric ceramics to continuously improve their dielectric properties [1–5]. Generally, low dielectric loss (tanδ, or high-quality factor $Q \times f$) can effectively suppress signal attenuation, near-zero temperature coefficient of resonance frequency (τ_f) can ensure the stability of electronic devices in extreme environments, and the appropriate relative permittivity (ε_r) not only regulates the signal delay but also ensures the miniaturization of electronic devices [6–8]. Among them, MWDCs with medium ε_r not only have lower dielectric loss, and τ_f is also smaller, it is a key member of microwave dielectric ceramics. For exam ple, $LnAlO_3$, (Zn,Sn)TiO_4, AM_2O_6, AMNd/TaO_4, Li_2O–MgO(ZnO)–TiO_2 systems, etc [9–15].

In recent years, the Li_2O–MgO(ZnO)–TiO_2 ternary system has been extensively investigated due to its structural diversity, and several microwave dielectric ceramics with medium ε_r have been developed [16,17]. Firstly, George et al. $Li_2Mg/ZnTi_3O_8$ ceramics with a spinel structure were synthesized, its dielectric properties are $\varepsilon_r = 27.2/25.6$, $Q \times f = 42{,}000/72{,}000$ GHz, and $\tau_f = +3.2/-11.2$ ppm/°C [18]. Subsequently, Zhou et al. successfully prepared spinel-structured $Li_2Mg_3Ti_4O_{12}$ ceramics with $\varepsilon_r = 20.2$, $Q \times f = 62{,}300$ GHz, and $\tau_f = -27.1$ ppm/°C by increasing the percentage of magnesium oxide [19]. Since then, a large number of researchers have used ionic substitution and non-stoichiometric modulation, both of which have been achieved to optimize the dielectric properties [8,15,20–22]. For the application of low-temperature co-sintering technology, a reduction in sintering temperature has been achieved by the addition of a wide variety of sintering additives [23–25]. Just recently, Tang et al. successfully prepared $Li_6M_7Ti_{11}O_{32}$ and $Li_{10}MTi_{13}O_{32}$ (M = Zn, Mg) dielectric ceramics with medium ε_r by further adjusting the ratio of the ternary system Li_2O–MgO (ZnO)–TiO_2. Among them, $Li_6Zn_7Ti_{11}O_{32}$ and $Li_6Mg_7Ti_{11}O_{32}$ exhibit ordered spinel structures with dielectric properties of $\varepsilon_r = 20.7$ and 21.9,

* Corresponding author.
** Corresponding author. School of Integrated Circuit Science and Engineering, University of Electronic Science and Technology of China, Chengdu, China.
*** Corresponding author. School of Electronic Science and Engineering, University of Electronic Science and Technology of China, Chengdu, 610054, China.
E-mail addresses: liukui96@163.com (K. Liu), dainanzhang@126.com (D. Zhang), hwzhang@uestc.edu.cn (H. Zhang).

https://doi.org/10.1016/j.ceramint.2024.01.164
Received 7 November 2023; Received in revised form 27 December 2023; Accepted 11 January 2024
Available online 21 January 2024

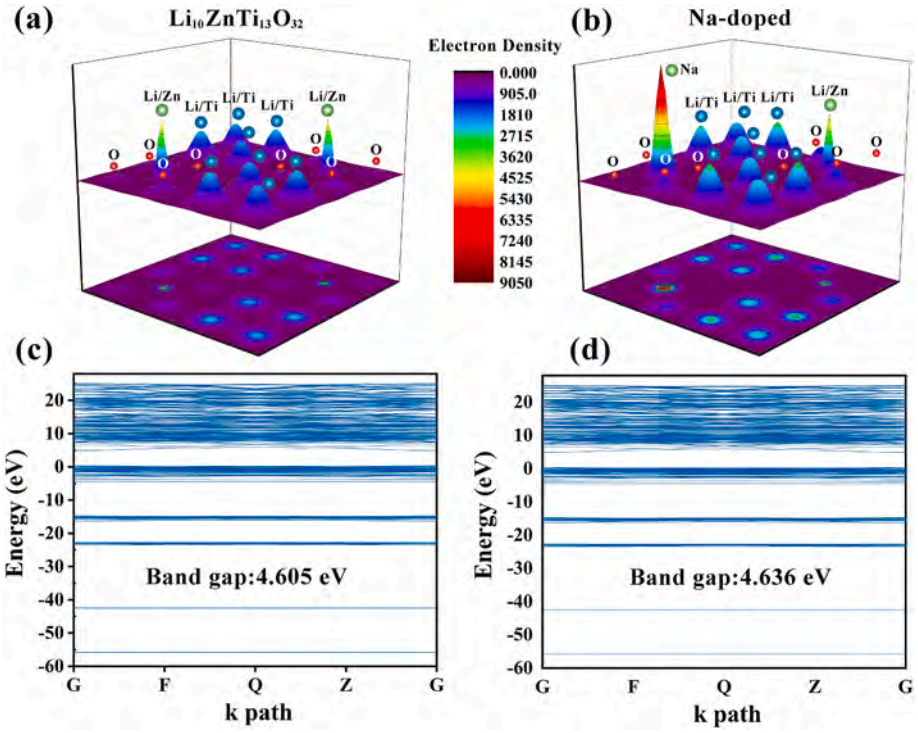

Fig. 1. Electron density and energy band structures of Na ions before and after doping.

$Q \times f$ = 129,600 GHz and 108,600 GHz, τ_f = −45 ppm/°C and −21 ppm/°C, respectively [26]. Whereas, $Li_{10}Zn/MgTi_{13}O_{32}$ exhibits disordered spinel structures, corresponding to dielectric properties of ε_r = 28.26/29.23, $Q \times f$ = 35, 800/32,100 GHz, and τ_f = −17.06/-11.05 ppm/°C. The occupancy of the different cations is a key factor in the change of ordering [16,27]. So far, no $Li_{10}MTi_{13}O_{32}$ (M = Zn, Mg) modification has been investigated, which is particularly important for further studies on the structure-property relationship of $Li_{10}MTi_{13}O_{32}$ (M = Zn, Mg).

In this work, it was shown by first-principles calculations that doping with Na ions will optimize the dielectric properties. Therefore, $Li_{(1-x)10}Na_{10x}ZnTi_{13}O_{32}$ ($0.004 \leq x \leq 0.020$) ceramics by solid-phase reaction method and the effect of non-intrinsic factors on their dielectric properties was elucidated by varying their relative density, grain size, and second phase content. The effect of intrinsic factors on the dielectric properties was revealed by analyzing the lattice vibrational properties.

2. Experiment

$Li_{(1-x)10}Na_{10x}ZnTi_{13}O_{32}$ ($0.004 \leq x \leq 0.020$) ceramics were prepared by a conventional solid phase reaction method. Li_2CO_3 (Aladdin, 99.99 %), Na_2CO_3 (Aladdin, 99.99 %), ZnO (Aladdin, 99.99 %), and TiO_2 (Aladdin, 99.8 %) powders were weighed and mixed in stoichiometric ratio. The powder was ball milled in a nylon ball milling jar for 10h, where the ball milling medium was deionized water and zirconium dioxide balls. Subsequently, the slurry was dried and calcined at 800 °C for 4 h. The calcined powder was ball milled for a second time for 10 h. The slurry obtained in the second time was dried and ground, and then granulated by adding 8 wt% polyvinyl alcohol (PVA) solution. The granulated particles were uniaxially pressed into cylindrical billets with a diameter of 12 mm and a height of 5–6 mm. Finally, the cylindrical raw billets were sintered at 500 °C for 2 h to achieve PVA removal and then sintered at 975–1000 °C for 4 h to densify the ceramics. The temperature change rate during the sintering process was 3 °C/min. The ceramic samples after sintering at 1050 °C were polished and then thermally etched at 1000 °C for 2 h with a temperature change rate of 5 °C/min. X-ray photoelectron spectroscopy (XPS, Thermo Scientific K-Alpha, USA) was used to analyze the chemical state of Ti and O in ceramic samples. Reflectance spectra were determined using a PerkinElmer Lambda950 UV–Vis spectrophotometer (USA).

First-principle calculations were carried out using the CASTEP module of Density Functional Theory (DFT), and the specific parameter settings used for the calculations are given in the Supplementary Information (SI). The bulk density of the ceramics was measured by the Archimedes drainage method. X-ray diffractometer (XRD, SmartLab 9 kW, Rigaku, Japan) was used to characterize the phase composition and crystal structure of the ceramics. Field emission scanning electron microscopy (FESEM, Phenom, fPharos, Netherlands) was used to analyze the microscopic morphology and elemental distribution of the samples. Raman spectroscopy with a wavenumber located between 50 cm^{-1} and 2000 cm^{-1} was examined by a Raman spectrometer (LabRAM HR evolution, Horiba Scientific, Japan) using a He–Ne laser as the excitation source. The microwave dielectric properties at frequencies between 2 GHz and 20 GHz were measured using a vector network analyzer (Agilent N5230A, Agilent Technologies, USA) in TE011 mode using the Hakki-Coleman dielectric resonator method, where τ_f was calculated using the formula shown below:

$$\tau_f = \frac{f_b - f_a}{(T_b - T_a) \times f_a} \times 10^6 \text{ ppm/°C} \quad (1)$$

where f_a and f_b represent the resonant frequency at T_a and T_b, respectively.

3. Results and discussions

3.1DFTcalculations

Before performing the experiments, we calculated the electron densities of the one-fifth unit cell before and after the substitution of Na ions for Li ions by first principles, as shown in Fig. 1(a)-(b). The doping of Na ions significantly enhances the density of the electron cloud inside the $[NaO_4]$ tetrahedron and causes the electron cloud inside the $[Li/TiO_6]$ octahedron to move towards the cation around the cation. Overall, the

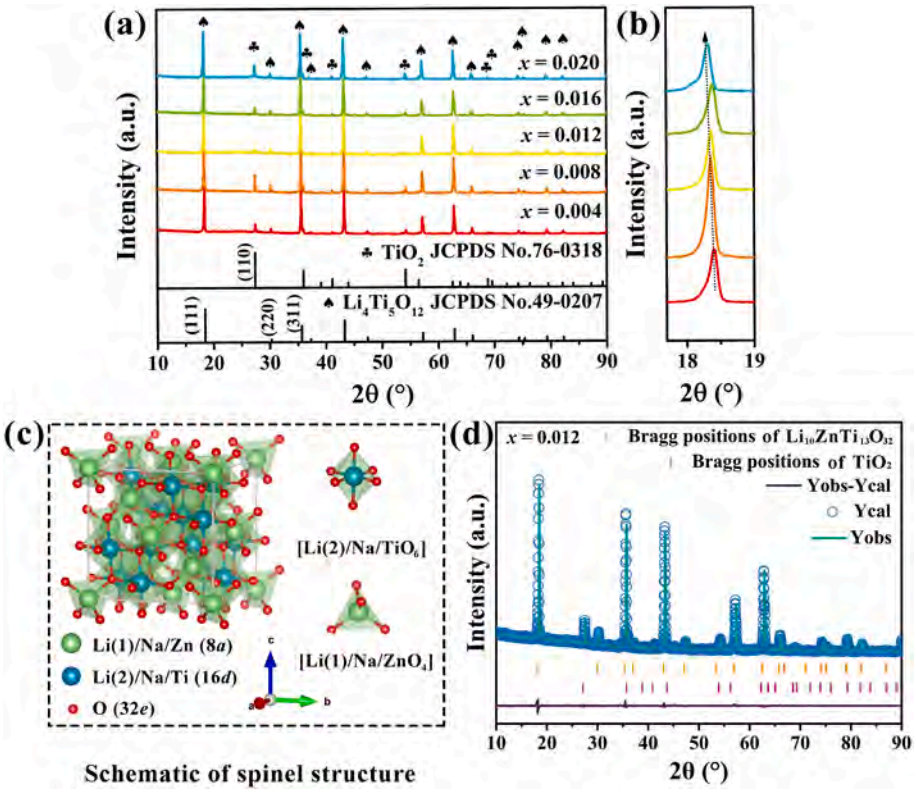

Fig. 2. (a) XRD patterns of $Li_{(1-x)10}Na_{10x}ZnTi_{13}O_{32}$ ceramics sintered at 1050 °C for 4 h. (b) Enlarged view of XRD patterns of the 2θ range between 18.5° and 19°. (c) Schematic of the crystal structure of $Li_{(1-x)10}Na_{10x}ZnTi_{13}O_{32}$ ceramics. (d) XRD refinement pattern for $x = 0.012$.

increase in the electron cloud density results in less energy available for lattice oscillations to overcome thermal losses, and thus fewer phonon collision losses, leading to a reduction in dielectric losses. The energy band structure before and after doping is shown in Fig. 1(c)–(d), where the band gap increases from 4.605 eV to 4.636 eV. This indicates that Na ion substitution leads to ceramics with lower conductivity loss, which also reduces the dielectric loss [13,28]. This suggests that doping with Na ions will optimize the dielectric properties.

3.2Crystalline structure

The XRD patterns of $Li_{(1-x)10}Na_{10x}ZnTi_{13}O_{32}$ ($0.004 \leq x \leq 0.020$) ceramics after sintering at 1050 °C for 4 h are shown in Fig. 2(a). The diffraction peaks of all component samples of $Li_{(1-x)10}Na_{10x}ZnTi_{13}O_{32}$ are a good match to the disordered spinel $Li_4Ti_5O_{12}$ (JCPDS#49–0207) with the *Fd-3m* (*227*) space group, but all samples also detected the secondary phase of TiO_2 (JCPDS#76–0318) with the $P4_2$ (*136*) space group. The secondary phase is inevitable due to the volatilization of lithium during high-temperature sintering of lithium-containing materials [29–32]. Fig. 2(b) shows the amplified pattern of the diffraction peak of (111). As the x value increases, the diffraction peak gradually moves towards the direction of decreasing 2θ, which is due to the lattice expansion caused by the substitution of Na^+. As shown in Fig. 2(c), the Na^+ substitution randomly occupies the *8a* Wyckoff position of the oxygen tetrahedron, and the *16d* Wyckoff position of the oxygen octahedron. When the coordination number is 4, the ionic radius of Na^+ is 0.99 Å, which is larger than that of Li^+ (0.59 Å), and when the coordination number is 6, the ionic radius of Na^+ is 1.02 Å, which is also larger than that of Li^+ (0.76 Å). Therefore, the substitution of Na+ is the main reason for the lattice expansion. To further investigate the effect of Na ion doping on the lattice parameters as well as the content of the second phase, Rietveld refinement of the XRD data was carried out by using GSAS software, and the refinement curves are plotted in Fig. 2(d) for $Li_{9.88}Na_{0.12}ZnTi_{13}O_{32}$, and those for the rest of the fractions are shown in Fig. S1. The refinement factors, lattice parameters, theoretical densities ($\rho_{th.}$), two-phase mass fractions, and main-phase bond lengths. The content of the secondary phase is least at $x = 0.012$, which indicates that a moderate amount of Na doping can reduce the generation of the secondary phase. The overall trend of change in cell volume shows a gradual increase, which echoes the above. Since the density of TiO_2 is higher than that of $Li_{(1-x)10}Na_{10x}ZnTi_{13}O_{32}$, the trend of density change is consistent with the change in TiO_2 content [33].

Table 1
The reliability factors, Weight fractions (W.f.), theoretical density, refined lattice parameters, and bond length of the main phase (*d*, unit: Å; A: $Li_{10}ZnTi_{13}O_{32}$; B: TiO_2.).

Projects	$x = 0.004$	$x = 0.008$	$x = 0.0012$	$x = 0.016$	$x = 0.020$
R_p (%)	5.56	5.87	6.33	4.98	6.68
R_{wp} (%)	8.06	8.39	9.38	7.01	9.78
χ^2	1.79	1.91	2.07	1.49	2.16
W.f. of A (%)	92.7	94.2	96.4	87.4	81.8
W.f. of B (%)	7.3	5.8	3.6	12.6	18.2
$a = b = c$ (Å)	8.3595	8.3610	8.3624	8.3653	8.3640
$\alpha = \beta = \gamma$ (°)	90	90	90	90	90
V (Å^3)	584.1744	584.5014	584.7866	585.3826	585.1162
$\rho_{th.}$(g/cm^3)	3.65	3.64	3.63	3.68	3.72
d-Li(1)/Na/Zn–O	1.9150	1.9599	1.9161	1.9527	1.9341
d-Li(2)/Na/Ti–O	2.0310	2.0075	2.0315	2.0129	2.0223

3.3. Lattice vibration properties

Lattice vibrational properties can effectively reflect the performance effects caused by chemical bonding changes, and Raman spectroscopy is

Table 2
Character Table of Irreducible Representations of $Li_{(1-x)10}Na_{10x}ZnTi_{13}O_{32}$.

D_{2h}	1	4	2_{100}	3	2_{110}	−1	−4	M_{100}	−3	M_{110}	Functions
$A_{1g}\Gamma_1^+$	1	1	1	1	1	1	1	1	1	1	x^2,y^2,z^2
$A_{1u}\Gamma_1^-$	1	1	1	1	1	−1	−1	−1	−1	−1	
$A_{2g}\Gamma_2^+$	1	−1	1	1	−1	1	−1	1	1	−1	
$A_{2u}\Gamma_2^-$	1	−1	1	1	−1	−1	1	−1	−1	1	
$E_g\Gamma_3^+$	2	0	2	−1	0	2	0	2	−1	0	$(2z^2-x^2-y^2, x^2-y^2)$
$E_u\Gamma_3^-$	2	0	2	−1	0	−2	0	−2	1	0	
$F_{2u}\Gamma_5^-$	3	−1	−1	0	1	−3	1	1	0	−1	
$F_{2g}\Gamma_5^+$	3	−1	−1	0	1	3	−1	−1	0	1	(xy, xz, yz)
$F_{1u}\Gamma_4^-$	3	1	−1	0	−1	−3	−1	1	0	1	(x, y, z)
$F_{2g}\Gamma_4^+$	3	1	−1	0	−1	3	1	−1	0	−1	yz,J_x

Table 3
Raman and IR vibrational modes of the $Li_{(1-x)10}Na_{10x}ZnTi_{13}O_{32}$ structure.

Atom	Position	Symmetry	Irreducible vibrational representations
Li(1)/Na/Zn	*8a*	T_d	$2F_{1u} + F_{2g}$
Li(2)/Na/Ti	*16d*	D_{3d}	$4F_{1u} + A_{2u} + E_u + F_{2u}$
O	*32e*	C_{3v}	$4F_{1u} + A_{1g} + E_g + 2F_{2g} + A_{2u} + E_u + F_{2u}$
$\Gamma_{Optic} = 10F_{1u} + A_{1g} + E_g + 3F_{2g} + 2A_{2u} + 2E_u + 2F_{2u}$			
$\Gamma_{acoustic} = F_{1u}$			
$\Gamma_{Raman} = 5F_{1u} + A_{1g} + E_g + 3F_{2g} + 2A_{2u} + 2E_u + 2F_{2u}$ (including Hyper-Raman active modes)			
$\Gamma_{Infrared} = 4F_{1u}$ (acoustic modes excluded)			

the main means to study lattice vibrational properties. According to the group theory analysis, the vibrational properties of the space group for the point groups *Fd-3m* (*227*) and O_h (*m3m*) are shown in Table 1, and the vibrational mode classifications are listed in Table 2. Theoretically, $Li_{(1-x)10}Na_{10x}ZnTi_{13}O_{32}$ should have 16 Raman vibrational modes, including the super-Raman active modes [34] (see Table 3).

The Raman spectra of $Li_{(1-x)10}Na_{10x}ZnTi_{13}O_{32}$ ceramics are shown in Fig. 3(a), with a total of nine Raman vibrational modes detected. Some Raman vibrational modes were not detected due to differences in Raman vibrational activity during the measurement process and background masking. In addition, it can be observed from Fig. 3(a) that the wavenumber and full width at half maxima (FWHM) of the Raman characteristic peaks change for different samples. To further carry out the assignment of Raman vibrational modes and to investigate the effect of lattice vibrational changes on the dielectric properties, the Raman spectra were fitted by Gauss-Lorentzian model as shown in Fig. 3(b) and Fig. S2. Among them, the Raman vibrational modes located between 200 cm^{-1} and 400 cm^{-1} are caused by the bending vibrations of O–Li/Na/Ti–O. The stretching vibrations of the [Li/NaO_4] tetrahedra produced vibrational modes located near 426 cm^{-1}, while the stretching vibrations of the [ZnO_4] tetrahedra caused vibrational modes located near 500 cm^{-1}. The vibrational mode located near 681 cm^{-1} is associated with the telescopic vibration of the [TiO_6] octahedron [27]. While the remaining unassigned vibrational modes are generated by the secondary phase of TiO_2 [35]. The effect of changes in lattice vibrational properties on dielectric properties will be analyzed later.

3.4Microstructures

Fig. 4 shows the microscopic morphology of thermally etched $Li_{(1-x)10}Na_{10x}ZnTi_{13}O_{32}$ ceramics with different compositions after sintering at 1050 °C. All the samples have a dense microstructure with distinct and easily recognizable grain boundaries. In addition, very few grain boundary pores exist at the grain boundaries. In addition, very few grain boundary pores exist at the grain boundaries. With the increase of Na^+ ion substitution, the average grain size showed a trend of increasing and then decreasing. The statistical distribution of grain size is shown in Fig. S3, where $Li_{9.88}Na_{0.12}ZnTi_{13}O_{32}$ has the highest average grain size of 5 μm. At this point, the porosity is also the lowest, at 4.21 %. Appropriate Na^+ substitution can promote the sintering of the ceramics, thus increasing the grain size and reducing the porosity. Fig. 5 shows the EDS characterization results for $x = 0.012$. A clear distinction between the two grains can be observed in the back-scattered electron imaging. The smaller and relatively brighter size grains are TiO_2, while the larger and relatively darker size grains are $Li_{9.88}Na_{0.12}ZnTi_{13}O_{32}$. This result echoes the XRD results, confirming that there is indeed a TiO_2 secondary phase. Fig. 6 shows the elemental distribution of $Li_{9.988}Na_{0.012}ZnTi_{13}O_{32}$ ceramics, where Ti elemental aggregation was not observed due to the low TiO_2 content of the secondary phase and the high titanium content of the primary phase.

3.5. Microwave dielectric properties

Usually, non-intrinsic and intrinsic factors are the two main reasons affecting microwave dielectric ceramics. Non-intrinsic factors are mainly the densification of the ceramics, grain size, the presence of a second phase, and other factors. Intrinsic factors mainly refer to atomic properties, chemical bonding properties, lattice vibrational properties, and other factors. In this work, we have analyzed the effect of intrinsic and non-intrinsic factors on the dielectric properties separately.

Fig. 6(a) and (b) correspond to ε_r and $Q \times f$ values of $Li_{(1-x)}$

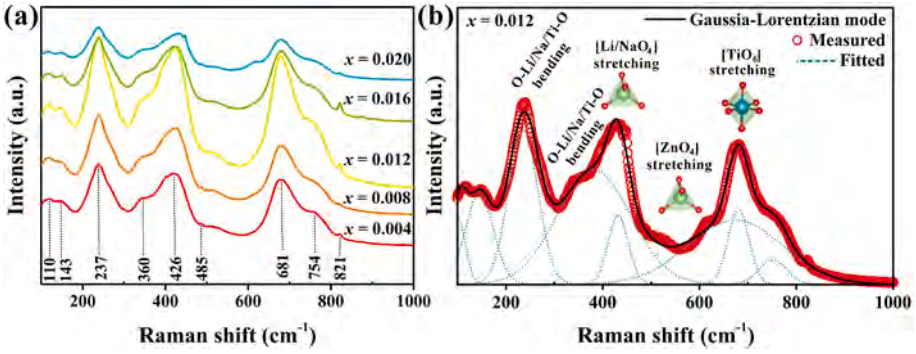

Fig. 3. (a) Raman spectra of $Li_{(1-x)10}Na_{10x}ZnTi_{13}O_{32}$ ceramics sintered at 1050 °C for 4 h. (b) The observed and fitted Raman Raman spectra at $x = 0.012$.

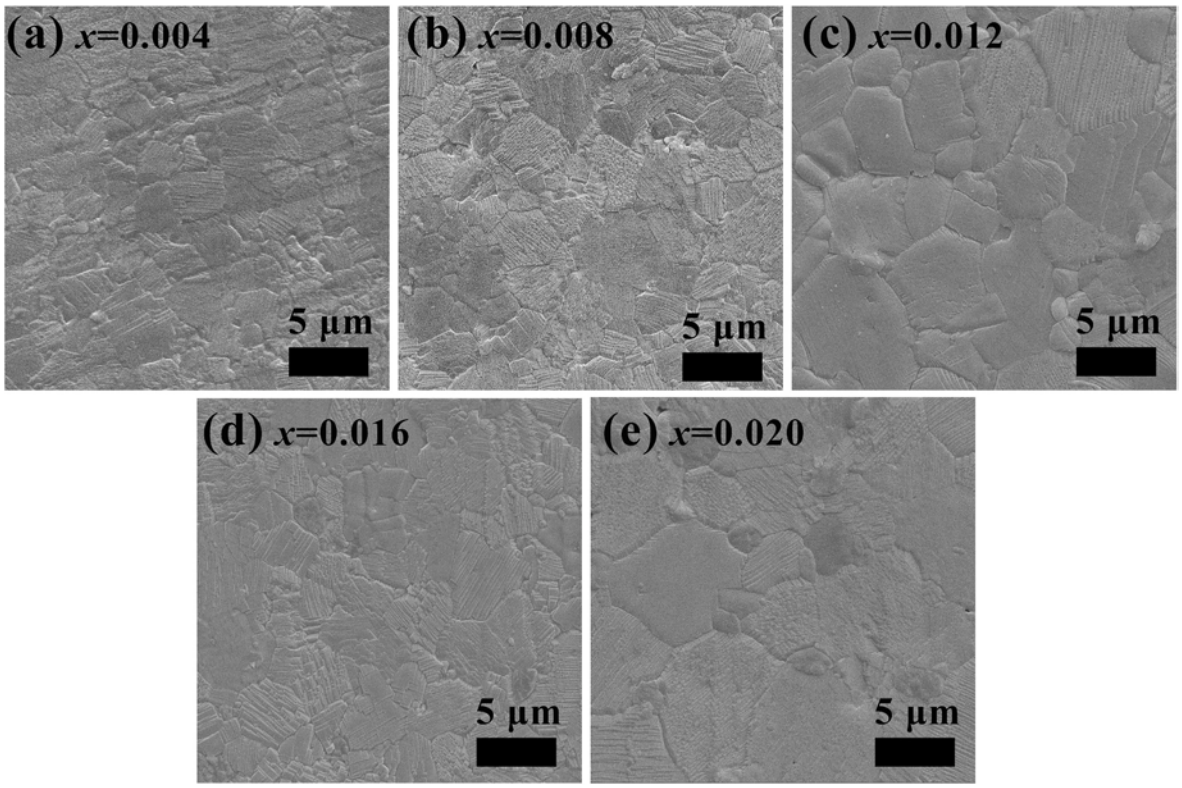

Fig. 4. (a)–(e) SEM micrographs of $Li_{(1-x)10}Na_{10x}ZnTi_{13}O_{32}$ ceramics after sintering at 1050 °C.

$_{10}Na_{10x}ZnTi_{13}O_{32}$ ceramics at different sintering temperatures, respectively. For samples with different compositions, ε_r, and $Q \times f$ both reach their maximum values at 1050 °C. Here, as the x value increases from 0.004 to 0.012, ε_r also increases from 28.77 to 29.53, and $Q \times f$ from 53,349 GHz to 90,879 GHz (@7.8 GHz). After that, ε_r continues to increase to 31.55 as the x value continues to increase to 0.020, while $Q \times f$ decreases to 44,396 GHz. The relative densities of all the samples are shown in Fig. 6(c), and the bulk densities are shown in Fig. S4. All the samples show excellent densities at 1050 °C, with the relative density of $Li_{9.88}Na_{0.12}ZnTi_{13}O_{32}$ reaching a maximum value of 98.19 %, which is responsible for its low dielectric loss. Fig. 6(d) summarizes the trends of ε_r, $Q \times f$, and relative density after sintering at 1050 °C for 4 h. In addition, the secondary phase TiO_2 has a high ε_r value, which also leads to an increase in the ε_r value of $Li_{(1-x)10}Na_{10x}ZnTi_{13}O_{32}$ ceramics [33]. Finally, Grain boundaries often act as two-dimensional defects that interrupt the long-range ordering of the crystal, leading to increased dielectric losses. SEM results show that $Li_{9.88}Na_{0.12}ZnTi_{13}O_{32}$ ceramic has the largest average grain size, and its reduced grain boundary density will help to reduce its dielectric loss.

For intrinsic factors, ion polarisation rate and lattice vibrational properties are the key factors affecting the dielectric properties. Fig. 7(a) plots the variation of observed permittivity ($\varepsilon_{r\text{-}obs.}$) and the corrected permittivity ($\varepsilon_{r\text{-}corr.}$) according to the Bosman-Havenga equation for the samples after sintering at 1050 °C [36].

$$\varepsilon_{r-corr.} = \varepsilon_{r-obs.}(1 + 1.5p) \tag{2}$$

The trends of the two changes remain consistent and gradually increase with the increase of Na ion doping. According to the Clausius-Mossotti equation [37]:

$$\varepsilon_{r-cal.} = \frac{3V + 8\pi\alpha}{3V - 4\pi\alpha} \tag{3}$$

It can be seen that ε_r is directly proportional to the ionic polarisability, which leads to an increase in ε_r since the ionic polarisability of Na^+ (1.80 $Å^3$) is higher than that of Li^+ (1.20 $Å^3$). Changes in the vibrational properties of the lattice will also lead to changes in the dielectric constant. It has been shown that ε_r is inversely proportional to the wave number (frequency) and the trend of phonon displacement is opposite to ε_r, as shown in the following relation:

$$\varepsilon(0,\xi,\kappa) = \frac{\Omega_P^2 \, exp\left[\lambda\left(E_0^F - \xi\right)\right]}{\omega(\xi,\kappa)} \tag{4}$$

Ω_P and ω are the plasma frequency and phonon frequency, respectively [38,39]. Fig. 7(a) also plots the change in wavenumber of the Raman characteristic peak located near 237 cm^{-1}, which decreases from 237.97 cm^{-1} to 234.55 cm^{-1}as the x value increases, which is the opposite trend to that of ε_r. This indicates that Na ion doping does affect the lattice vibration, which causes ε_r to change.

Fig. 7(b) shows the variation curves of $Q \times f$ for $Li_{(1-x)10}Na_{10x}ZnTi_{13}O_{32}$ ceramics after sintering at 1050 °C. $Q \times f$ shows an increasing and then decreasing trend with the increase of x value. In addition, Fig. 7 (b) plots the variation of r full width at half maximum (FWHM) of the Raman characteristic peak located near 237 cm^{-1}. Since the dielectric loss is inversely proportional to the long-term attenuation of microwave energy transmission, this can be reflected by the lattice vibration variation. A smaller FWHM of the Raman characteristic peak implies that a certain type of vibrational mode has a lower damping behavior, which leads to a lower intrinsic dielectric loss [22]. The FWHM value decreases from 85.7 cm^{-1} to 71.9 cm^{-1}, and increases again to 88.6 cm^{-1}, and is minimum at $x = 0.012$. This suggests that the proper substitution of Na ions reduces the vibrational damping behavior of the O–Li/Na/Ti–O bond, which results in a reduction of the intrinsic loss. In addition, the chemical state of Ti in $Li_{9.88}Na_{0.12}ZnTi_{13}O_{32}$ ceramics was analyzed by XPS, as shown in Fig. S6. The presence of Ti^{3+} was not observed, indicating that the enhancement of the anharmonic vibration by the reduction of Ti^{4+} to Ti^{3+} during sintering to reduce the value of $Q \times f$ does not exist.

As a substrate material for electronic devices, good temperature stability is an essential requirement for microwave dielectric ceramics.

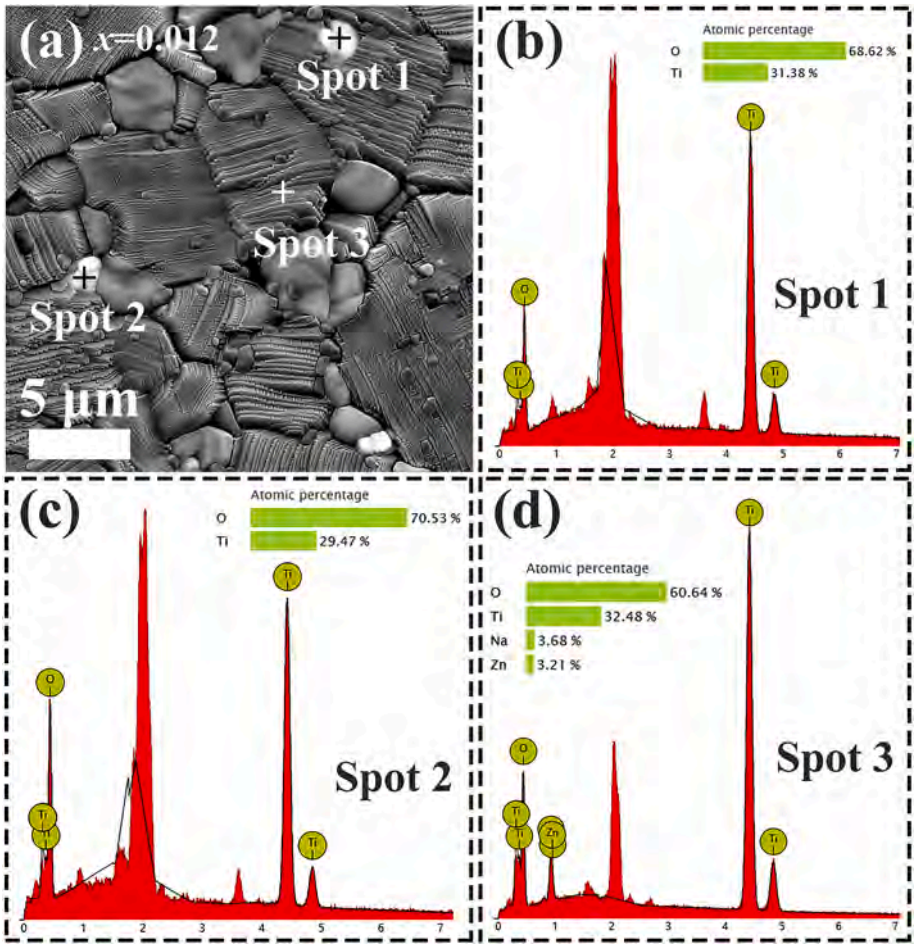

Fig. 5. EDS results of $Li_{9.88}Na_{0.12}ZnTi_{13}O_{32}$ ceramics sintered at 1050 °C for 4 h.

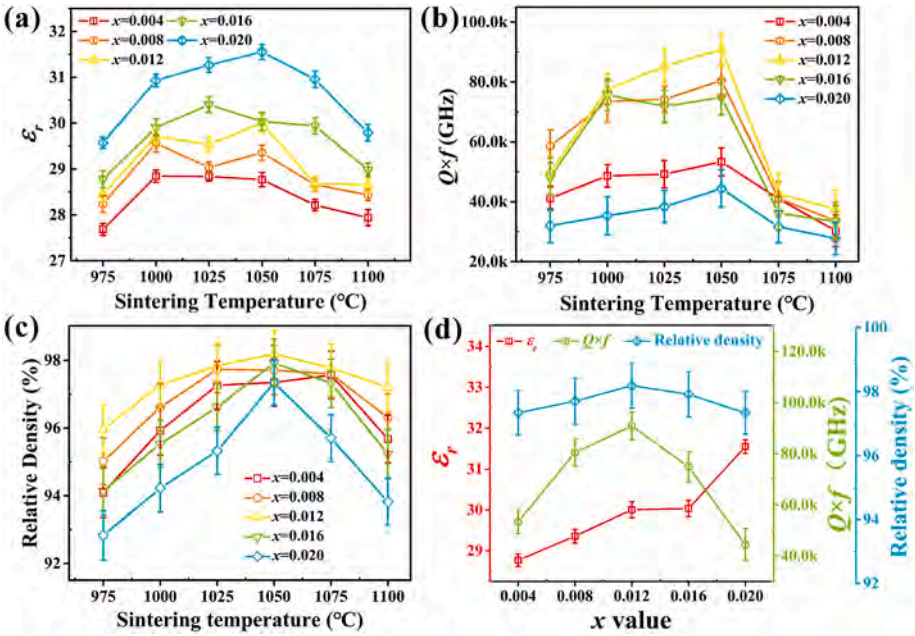

Fig. 6. (a)–(c) ε_r, $Q \times f$, and relative density of $Li_{(1-x)10}Na_{10x}ZnTi_{13}O_{32}$ ceramics at different sintering temperatures. (d) Comparison chart of relative density, dielectric constant, and quality factor at 1050 °C for different contents.

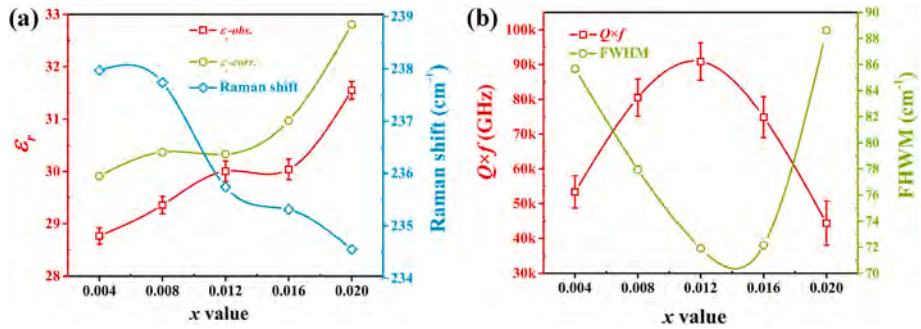

Fig. 7. (a) The $\varepsilon_{r\text{-obs.}}$, $\varepsilon_{r\text{-corr.}}$, and characteristic peak shifts of $\varepsilon_{r\text{-cal.}}$ of $Li_{(1-x)10}Na_{10x}ZnTi_{13}O_{32}$ sintered at 1050 °C for 4 h. (b) The $Q \times f$ and FWHM curves of $Li_{(1-x)10}Na_{10x}ZnTi_{13}O_{32}$ sintered at 1050 °C for 4 h.

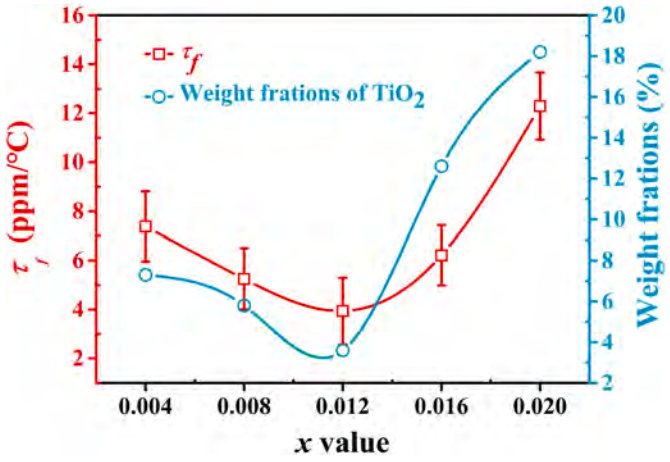

Fig. 8. τ_f values and weight fractions of the second phase of $Li_{(1-x)10}Na_{10x}ZnTi_{13}O_{32}$ ceramics after sintering at 1050 °C.

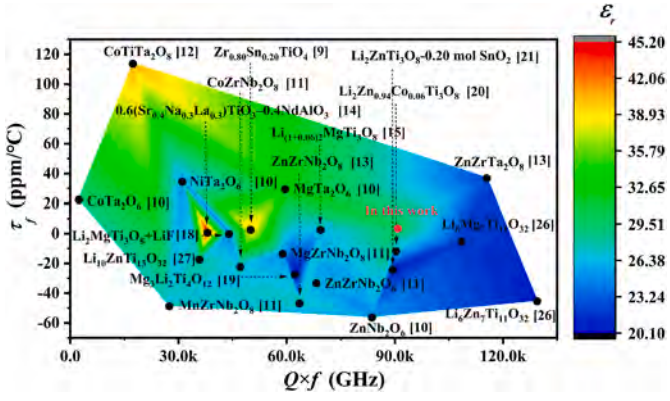

Fig. 9. Microwave dielectric properties of some of the reported ceramics with medium permittivity.

Usually, a τ_f value close to 0 ppm/°C represents better temperature stability. Fig. 8 shows the τ_f values of $Li_{(1-x)10}Na_{10x}ZnTi_{13}O_{32}$ ceramics after sintering at 1050 °C. With the gradual increase of the x value, the τ_f first decreases from 7.37 ppm/°C to 3.93 ppm/°C before increasing to 12.29 ppm/°C. This is superior to the reported τ_f of $Li_{10}ZnTi_{13}O_{32}$ ceramics (−17.06 ppm/°C) [27]. This is mainly attributed to the production of secondary phase TiO_2. Since TiO_2 has a large τ_f value of about 200 ppm/°C [33]. According to the law of mixing ($\tau_f = V_1 \times \tau_{f1} + V_2 \times \tau_{f2}$) [40], the τ_f value increases gradually with the increase in the content of TiO_2. Fig. 8 also limits the weight fractions of TiO_2 for the different components, which is the smallest at $x = 0.012$, when the temperature stability is the best, with a tf value of 3.93 ppm/°C.

Fig. 9 shows the microwave dielectric properties that have been reported for some ceramics with medium permittivity [9–15,18–21,26,27]. Na ion-doped $Li_{9.88}Na_{0.12}ZnTi_{13}O_{32}$ ceramic exhibits more excellent microwave dielectric properties among the family of ceramics with medium permittivity, especially with more excellent temperature stability. Fig. S7 also shows the UV–Vis spectra of the $Li_{9.88}Na_{0.12}ZnTi_{13}O_{32}$ ceramic, which has strong absorption in the UV region. This suggests that the modified $Li_{9.88}Na_{0.12}ZnTi_{13}O_{32}$ has a promising application in microwave communications.

4. Conclusion

In this work, first-principles calculations show that Na ion substitution contributes to the reduction of dielectric loss in $Li_{10}ZnTi_{13}O_{32}$ ceramics. $Li_{(1-x)10}Na_{10x}ZnTi_{13}O_{32}$ ceramics were prepared by solid-phase reaction method to establish the relationship between structure and properties. $Li_{9.88}Na_{0.12}ZnTi_{13}O_{32}$ exhibits the best dielectric properties $\varepsilon_r = 30.01$, $Q \times f = 90{,}879$ GHz (@7.8 GHz), $\tau_f = 3.93$ ppm/°C. For the non-intrinsic factors, the relative density is enhanced to 98.19 %, an increase in grain size to 5 μm, and an appropriate second phase content (TiO_2, 3.6 %) led to the optimization of the dielectric properties. For the intrinsic factors, the weakening of the damping properties and the increase in the electron cloud density lead to a decrease in the dielectric loss. The increase in ion polarisation and the blue shift of the Raman wave number lead to a gradual increase in ε_r. TiO_2 with more positive τ_f allows the optimization of temperature stability. The above results indicate that $Li_{9.88}Na_{0.12}ZnTi_{13}O_{32}$ ceramics have a wide application prospect in the field of microwave communications.

Declaration of competing interest

The authors declare that they have no known competing financial interests or personal relationships that could have appeared to influence the work reported in this paper.

Acknowledgments

We sincerely appreciate the projects supported by the National Natural Science Foundation of China (Grant No. 62271106, Grant No. 52372102), the National Key Scientific Instrument and Equipment Development Project (Grant No. 51827802), the Major Science and Technology Specific Projects of Sichuan Province (Grant No. 2019ZDZX0026), and the Natural Science Foundation of Sichuan Province (Grant No. 2022NSFSC0485).

Appendix A. Supplementary data

Supplementary data to this article can be found online at https://doi.org/10.1016/j.ceramint.2024.01.164.

References

[1] M.T. Sebastian, R. Ubic, H. Jantunen, Low-loss dielectric ceramic materials and their properties, Int. Mater. Rev. 60 (2015) 392–412.

[2] O. Elijah, C.Y. Leow, T.A. Rahman, S. Nunoo, S.Z. Iliya, A Comprehensive Survey of Pilot Contamination in massive MIMO—5G system, IEEE Commun. Surv. Tutorials 18 (2016) 905–923.

[3] K. Xiao, L. Gong, M. Kadoch, Opportunistic Multicast NOMA with Security Concerns in a 5G massive MIMO system, IEEE Commun. Mag. 56 (2018) 91–95.

[4] H.R. Tian, J.J. Zheng, L.T. Liu, H.T. Wu, H. Kimura, Y.Z. Lu, Z.X. Yue, Structure characteristics and microwave dielectric properties of $Pr_2(Zr_{1-x}Ti_x)_3(MoO_4)_9$ solid solution ceramic with a stable temperature coefficient, J. Mater. Sci. Technol. 116 (2033) 121-129..

[5] J. Bao, Y.P. Zhang, H. Kimura, H.T. Wu, Z.X. Yue, Crystal structure, chemical bond characteristics, infrared reflection spectrum, and microwave dielectric properties of $Nd_2(Zr_{1-x}Ti_x)_3(MoO_4)_9$ ceramics, J. Mater. Chem. C 5 (2017) 10094–10098.

[6] D. Zhou, L.X. Pang, D.W. Wang, C. Li, B. Jin, I.M. Reaney, High permittivity and low loss microwave dielectrics suitable for 5G resonators and low temperature co-fired ceramic architecture, J. Mater. Chem. C 5 (2017) 10094–10098.

[7] H. Yamada, T. Okawa, Y. Tohdo, H. Ohsato, Microwave dielectric properties of $Ba_xLa_4Ti_{3+x}O_{12+3x}$ (x = 0.0–1.0) ceramics, J. Eur. Ceram. Soc. 26 (2006) 2059–2062.

[8] K. Liu, L. Shi, X.Y. Wang, C. Liu, J. Li, Y.L. Liao, L.C. Jin, D.N. Zhang, H.W. Zhang, Li^+ enrichment to improve the microwave dielectric properties of $Li_2ZnTi_3O_8$ ceramics and the relationship between structure and properties, J. Eur. Ceram. Soc. 43 (2023) 1483–1491.

[9] S. Hirano, T. Hayashi, A. Hattori, Chemical processing and microwave characteristics of (Zr, Sn)TiO_4 microwave dielectrics, J. Am. Ceram. Soc. 74 (1991) 1320–1324.

[10] H.J. Lee, I. Kim, K.S. Hong, Dielectric properties of AB_2O_6 Compounds at microwave frequencies (A=Ca, Mg, Mn, Co, Ni, Zn, and B=Nb, Ta), Jpn. J. Appl. Phys. 36 (1997) L1318.

[11] H.T. Wu, Z.B. Feng, Q.J. Mei, J.D. Guo, J.X. Bi, Correlations of crystal structure, bond energy and microwave dielectric properties of $AZrNb_2O_8$ (A = Zn, Co, Mg, Mn) ceramics, J. Alloy. Compd. 648 (5) (2015) 368–373.

[12] H. Yang, S. Zhang, Y. Chen, H. Yang, Y. Yuan, E. Li, Crystal Chemistry, Raman spectra, and bond characteristics of Trirutile-type $Co_{0.5}Ti_{0.5}TaO_4$ microwave dielectric ceramics, Inorg. Chem. 58 (1) (2018) 968–976.

[13] K. Liu, H.W. Zhang, C. Liu, L. Shi, X.Y. Wang, J. Li, Y.L. Liao, D.N. Zhang, Structure evolution of wolframite-type $ZnZrC_2O_8$ (C = Nb, Ta) ceramics in relation to microwave dielectric properties, J. Am. Ceram. Soc. 106 (2023) 1089–1101.

[14] F. Liu, X.Y. Liu, C.L. Yuan, J.J. Qu, G.H. Chen, C.R. Zhou, F. Liu, Microstructures and microwave dielectric properties of $(1-x)(Sr_{0.4}Na_{0.3}La_{0.3})TiO_3$–$xLnAlO_3$ (Ln=Sm, Nd) ceramic systems, J. Eur. Ceram. Soc. 45 (2015) 2091–2098.

[15] K. Liu, C. Liu, J. Li, L.C. Jin, H.W. Zhang, Relationship between structure and properties of microwave dielectric ceramic $Li_{(1+x)2}MgTi_3O_8$ based on Li non-stoichiometry, J. Materiomics 9 (2023) 279–288.

[16] V.S. Hernandez, L.M.T. Martinez, G.C. Mather, A.R. West, Stoichiometry, structures and polymorphism of spinel-like phases, $Li_{1.33x}Zn_{2-2x}Ti_{1+0.67x}O_4$, J. Mater. Chem. 6 (1996) 1533–1536.

[17] J. Zhang Jian, R.Z. Zuo, Effect of ordering on the microwave dielectric properties of spinel-structured $(Zn_{1-x}(Li_{2/3}Ti_{1/3})_x)_2TiO_4$ ceramics, J. Am. Ceram. Soc. 99 (2016) 3343–3349.

[18] S. George, M.T. Sebastian, Low-temperature sintering and microwave dielectric properties of $Li_2ATi_3O_8$ (A=Mg, Zn) ceramics, Int. J. Appl. Ceram. Tec. 8 (2011) 1400–1407.

[19] H.F. Zhou, X.B. Liu, X.L. Chen, L. Fang, Preparation, phase structure and microwave dielectric properties of a new low cost $MgLi_{2/3}Ti_{4/3}O_4$ compound, Mater. Chem. Phys. 137 (2012) 22–25.

[20] X.P. Lu, Z.W. Dong, Y. Zheng, The relationships between structures and microwave dielectric properties of $Li_2Zn_{1-x}Co_xTi_3O_8$ ceramics, J. Electron. Mater. 46 (2017) 6977–6983.

[21] P. Zhang, Y.G. Zhao, High-Q microwave dielectric materials of $Li_2ZnTi_3O_8$ ceramics with SnO_2 additive, Ceram. Int. 42 (2016) 2882–2886.

[22] K. Xiao, Y. Tang, Y. Tian, C. Li, L. Duan, L. Fang, Enhancement of the cation order and the microwave dielectric properties of $Li_2ZnTi_3O_8$ through composition modulation, J. Eur. Ceram. Soc. 39 (2019) 3064–3069.

[23] H.S. Ren, L. Hao, H.Y. Peng, M.Z. Dang, T.Y. Xie, Y. Zhang, S.H. Jiang, X.G. Yao, H. X. Lin, L. Luo, Investigation on low-temperature sinterable behavior and tunable dielectric properties of BLMT glass-$Li_2ZnTi_3O_8$ composite ceramics, J. Eur. Ceram. Soc. 38 (2018) 3498–3504.

[24] X. Lu, Y. Zheng, Z. Dong, P. Cheng, R. Lin, Low temperature sintering and microwave dielectric properties of $Li_2ZnTi_3O_8$ ceramics doped with ZnO–La_2O_3–B_2O_3 glass, Ceram. Int. 40 (2014) 7087–7092.

[25] H.S. Ren, S.H. Jiang, M.Z. Dang, T.Y. Xie, H. Tang, H.Y. Peng, H.X. Lin, L. Luo, Investigating on sintering mechanism and adjustable dielectric properties of BLMT glass/$Li_2Zn_3Ti_4O_{12}$ composites for LTCC applications, J. Alloy. Compd. 740 (2018) 1188–1196.

[26] M. Li, Y. Tang, H.C. Xiang, J. Li, D. Zhou, L. Fang, Combined effect of rattling and compression on the microwave dielectric properties of B-site 1:3 ordered $Li_6A_7Ti_{11}O_{32}$ (A = Zn, Mg) spinels, Ceram. Int. 49 (2023) 8754–8761.

[27] Y. Tang, M. Li, H.C. Xiang, J. Li, Y.D. Qin, L. Fang, Mechanism of ionic polarizability, bond valence, and crystal structure on the microwave dielectric properties of disordered $Li_{10}MTi_{13}O_{32}$ (M = Zn, Mg) spinels, Materials Advances 4 (2023) 1345–1353.

[28] K. Kui, D.N. Zhang, Y.R. Yang, Q.S. Yin, Y.D. Lei, C. Liu, J. Li, L.C. Jin, Y.L. Liao, H. W. Zhang, Sintering behavior, structural evolution, and dielectric properties of $Li_{2+x}MgTiO_4F_x$ microwave dielectric ceramics, J. Eur. Ceram. Soc. 43 (2023) 6098–6106.

[29] G.G. Yao, X.S. Hu, X.L. Tian, P. Liu, J.P. Zhou, Synthesis and microwave dielectric properties of Li_2MgTiO_4 ceramics, Ceram. Int. 41 (2015) S563–S566.

[30] W.X. Que, L. Zhang, X. Yao, Y. Zhou, Y.L. Lam, Y.C. Chan, C.H. Kam, The effect of annealing atmosphere on structure characteristics of magnesium diffused lithium niobate single crystal substrates, Ferroelectrics 229 (1999) 249–254.

[31] C.S. Wu, K. Liu, H.L. Lai, F. Xu, Relationship between structure and microwave dielectric properties of $Li_3Mg_4Nb_{1-x}Ta_xO_8$ ceramics, J. Materiomics. (2023).

[32] K. Liu, Y.R. Yang, D.N. Zhang, L. Shi, X.Y. Wang, Q.S. Yin, C. Liu, J. Li, Y.L. Liao, H. W. Zhang, Effect of excess lithium on the structure and microwave dielectric properties of $LiMg_{0.5}Ti_{0.5}O_2$ ceramics, J. Am. Ceram. Soc. 106 (2023) 4794–4805.

[33] Z.Z. Weng, C. Wu, Z.X. Xiong, Y. Feng, H. AminiRastabi, C.X. Song, H. Xue, Low temperature sintering and microwave dielectric properties of TiO_2 ceramics, J. Eur. Ceram. Soc. 37 (2017) 4667–4672.

[34] D.L. Rousseau, R.P. Bauman, S.P. S Porto, Normal mode Determination in crystals, J. Raman Spectrosc. 10 (1981) 253–290.

[35] J.J. Jasinski, M. Lubas, K. Suchorab, M. Gawęda, L. Kurpaska, M. Brykala, A. Kosinska, M. Sitarz, J. Jagielski, Qualitative and semi-quantitative phase analysis of TiO_2 thin layers by Raman imaging, J. Mol. Struct. 1260 (2022) 132803.

[36] A.J. Bosman, E.E. Havinga, Temperature dependence of dielectric constants of Cubic ionic Compounds, Phys. Rev. 129 (1963) 1593–1600.

[37] P.V. Rysselberghe, Remarks concerning the Clausius-Mossotti law, J.phys.chem. 36 (1931) 1152–1155.

[38] F. Shi, H.L. Dong, Correlation of crystal structure, dielectric properties and lattice vibration spectra of $(Ba1_{-x}Sr_x)(Zn_{1/3}Nb_{2/3})O_3$ solid solutions, Dalton T 40 (2011) 6659–6667.

[39] A.D. Arulsamy, Renormalization group method based on the ionization energy theory, Ann. Phys. 326 (2011) 541–565.

[40] D.W. Kim, B. Park, J.H. Chung, K.S. Hong, Mixture behavior and microwave dielectric properties in the low-fired TiO_2–CuO system, Jpn. J. Appl. Phys. 39 (2000) 2696.